Investigation of Some Physical Properties of Cobalt Doped MoO_3 Nanofilms and Their Effects on the Degradation of the Methylene Blue Solution under UV Illumination

N. Benameur, A. Boukhachem, M. Ghamnia, M. A. Chakhoum, M. A. Dahamni, and C. Fauquet

***Abstract*—Pristine and Cobalt (Co)-doped MoO_3 nanofilms were synthesized on glass substrates using the spray pyrolysis method. The nanometric pristine MoO_3 films were prepared from the 10^{-2} $M.L^{-1}$ solution of ammonium molybdate tetrahydrate $[(NH_4)_6Mo_7O_{24},4H_2O]$ in distilled water. Co-doping at 0.5, 0.75 and 1% was obtained by adding cobalt (II) chloride hexahydrate ($Cl_2CoH_{12}O_6$) in the pristine solution. The structure and the morphology of the films were investigated by X-ray diffraction and atomic force microscopy. Two pronounced (020) and (040) peaks corresponding to the orthorhombic structure phase of α-MoO_3 were detected. The AFM observations showed the formation of micro-plates parallel to the surface plane with a roughness ranging from 33 nm to 54 nm. Optical properties were investigated through reflectance, transmittance and photoluminescence measurements. The optical band gap, the Urbach energy and the refractive index were deduced from these measurements. The presence of oxygen vacancies were revealed from the interband transitions in the blue and green domains. Co-doped MoO_3 nanofilms showed ferromagnetic behavior. Photocatalytic degradation of aqueous solution of methylene blue (MB) under UV irradiation in the presence of Co-MoO_3 nanofilms has been carried out using UV-visible spectrometer by monitoring the absorption of the solution of MB. The intensity of the absorption peak recorded toward 660 nm was deceased with the increase of the UV-illumination time and the color of the initial MB solution was drastically degraded.**

***Index Terms*—MoO_3 nanofilms, magnetic properties, optical properties, photocatalytic properties, spray pyrolysis method.**

I. Introduction

Transition metal oxide semiconductors (TMOs) such as TiO_2, WO_3, MoO_3, have been the subject of extended studies because of their applications in various domains [1]-[4], due to their interesting physical properties. Some of these materials are already used in environmental applications [5]-[8] and tested in many photocatalytic degradation such as phenol, methyl orange, rhodamine B and methyl Blue [9]-[12].

Manuscript received February 2019; revised April 4, 2019.

N. Benameur is with Laboratoire des Sciences de la Matière Condensée (LSMC), Université Oran 1 Ahmed Ben Bella, Algeria (e-mail: nadir.benameur@yahoo.fr).

A. Boukhachem is with El Manar University of Tunis, 2092 Tunis, Tunisia (e-mail: abdelwahab.boukhachem@laposte.net).

M. Ghamnia, M. A. Chakhoum, and M. A. Dahamni are with Laboratory of the Sciences of Condensed Matter, University of Oran 1 Ahmed Ben Bella, Algeria (e-mail: mghamnia@yahoo.fr, chakhoumali@gmail.com).

C. Fauquet is with Centre Interdisciplinaire de Nanoscience de Marseille, University of Marseille, Campus of Luminy, 13288, Marseille, France.

MoO_3, which is a wide bandgap n-type semiconductor, is of interest for applications. This oxide can exist under three phases [13]-[16]:

i. α-MoO_3 phase which is a promising oxide is thermodynamically stable

ii. β-MoO_3 and h-MoO_3 which constitute metastable phases

Due to its high stability, α-MoO_3 is considered as a potential candidate for photocatalysis applications [17], [18].

The growth and the synthesis of MoO_3 thin can be achieved via MOCVD [19], Chemical Vapor Deposition (CVD) [20], sputtering [21], Pulsed Laser ablation (PLD), vacuum evaporation [22] and spray pyrolysis [23]-[26]. Spray pyrolysis, which is a cheaper and easier method to implement, has been widely used to synthesize MoO_3 films [27], [28].

In order to improve some physical proprieties, MoO_3 was doped by various elements such as: tin [27], cobalt [29], tungsten [30], erbium [31], zinc [32], europium [17] and cadmium [33]. Cobalt is interesting due to its magnetic properties and for the behavior of the catalytic MoO_3-layers under UV irradiation. For its applications in the environment domain, this material has been applied in the photocatalysis of Methylene Blue (MB) [34], [35].

Yang Liu *et al* [36] have synthesized porous monoliths of MoO_3 nanoplates which were obtained from ammonium molybdate by freeze-casting and subsequent thermal treatment, a good photocatalytic activity for photodegradation of MB have been shown. Likewise, M. Szkoda *et al*. [37], [38] studied photocatalytical properties of MoO_3 microstructures obtained via an electrochemical anodization technique.

In recent works, photocatalytic activity of the both α-MoO_3 and h-MoO_3 phases was studied.

A. Chithambararaj *et al*. [39] found that the h-MoO_3 phase gives a photocatalytic response under visible light better than α-MoO_3 one. Nanobelts of single crystalline MoO_3 prepared by hydrothermal method show a high photodegradation of methylene blue under visible light illumination [40].

In this context, the aim of this paper is to synthesize MoO_3 thin films using a spray pyrolysis technique and to study the effect of the Co-doping low concentrations on some properties of α-MoO_3 thin films. Pristine and doped MoO_3 thin films were studied using XRD, optical reflectance and transmission spectra, PL measurements and atomic force microscopy. The magnetic behavior of Co-MoO_3 nanometric films and its surface photocatalytic activities are presented and discussed.

doi: 10.18178/ijcea.2019.10.2.736

II. Experimental Procedure

A. Synthesis of Pristine and Co-doped MoO_3 Films

Pristine and Co-doped α-MoO_3 nanofilms were synthesized by the spray pyrolysis method from a 10^{-2}M.L^{-1} solution concentrated of ammonium molybdate tetrahydrate [$(NH_4)_6Mo_7O_{24}$, $4H_2O$] in distilled water. By adding different weights of cobalt chloride hexahydrate ($CoCl_2$, $6H_2O$) in the initial solution, we have obtained Co-doped MoO_3 nanofilms. The (Co/Mo) molar ratios used were 0.5, 0.75, and 1 % respectively. The samples were characterized and analyzed by different techniques as described in the following paragraph.

B. Characterization Techniques

The crystallographic structure of the films was analyzed by X-ray diffraction (Philips PW 1729 with Cu-K_α radiation λ= 1.5406 Å). The surface morphologies were observed by atomic force microscopy (AFM-Dimension Edge version from Bruker) using tapping mode. The optical transmittance T(λ) and reflectance R(λ) were recorded in the 300-2000 nm wavelength range using a Shimadzu UV 3100 double-beam spectrophotometer. The photoluminescence measurements were carried out at room temperature using a Perkin Elmer spectrometer with a laser wavelength of 270 nm. The magnetic properties were recorded by the study of hysteresis loops: room temperature measurements of the magnetization as a function of the magnetic field was recorded on a Vibrating Sample Magnetometer (VSM) unit. The degradation of the absorption of the solution was monitored and observed in real time by immersing the samples in a beaker containing a methylene blue solution concentrated at 5 mg.L^{-1} under UV illumination (power 20 W, wavelength 253.7 nm).

III. Results and Discusions

A. Structural and Morphological Properties of MoO_3 Nanofilms

Fig. 1 shows the X-ray diffraction patterns of Co-doped MoO_3 films with different doping levels. One can observe from this figure, that all the diffraction peaks: (020), (040), (131) and (261) correspond to the diffraction of the orthorhombic planes of α-MoO_3 phase (JCPDS N°: 76-1003 card). Moreover, the XRD spectra of Co-doped or undoped MoO_3 films show a pronounced diffraction peaks (020) and (040) indicating a preferential orientation of MoO_3 crystallites along these directions. No secondary peak related to Co oxide or to others phases were observed, confirming that the synthesized films are pure orthorhombic MoO_3.

Before irradiation, the solution was stirred in the dark for 30 min to ensure the establishment of an adsorption–desorption equilibrium. The degradation of the absorption spectrum of the solution was recorded every 30 min.

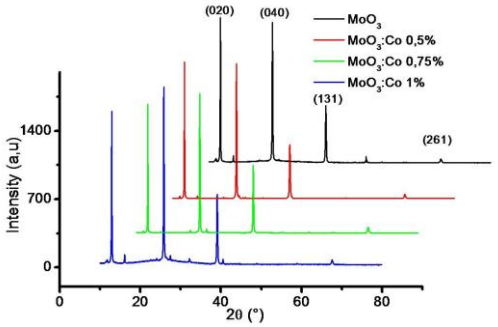

Fig. 1. X-ray diffraction spectra of Pristine and Co-doped MoO_3 thin films.

In addition, the exploitation of XRD spectra allowed us to determine some crystalline parameters such as the interplanar spacing d_{hkl} or the lattice parameters.

The interplanar spacing d_{hkl} values were determined from the Bragg equation :

$$2d_{hkl}\sin\theta = n\lambda \quad (1)$$

The interplanar spacing d_{hkl} values are depending on Miller indices *h*, *k*, *l* and lattice parameters by the following relation:

$$\frac{1}{d_{hkl}^2} = \frac{h^2}{a^2} + \frac{l^2}{b^2} + \frac{l^2}{c^2} \quad (2)$$

The calculated lattice constants are listed in the following table.

TABLE I: Lattice Parameters of Pristine and Co-doped MoO_3 Nanofilms Obtained from XRD Spectra

	a (Å)	b (Å)	c (Å)	b/a	b/c	c/a	V (Å^3)
Pristine MoO_3	3.8386	13.7774	3.7150	3.59	3.71	0.97	196.471
Co-MoO_3 (0.5%)	3.9806	13.7021	3.5900	3.44	3.82	0.90	195.808
Co-MoO_3 (0.75%)	3.9663	13.7787	3.6112	3.47	3.81	0.91	197.354
Co-MoO_3 (1%)	3.8399	13.7404	3.7125	3.58	3.70	0.97	195.878

From these values, we note that the lattice parameters are strongly depending on cobalt doping levels. The minimum value of *c/a* = 0.90 was obtained for 0.5% Co-doped while the greatest value 0.97 is recorded for the Co-doping of 0.75%. This can give a particular compactness and it is probably at the origin of the magnetic behavior of the Co-doping MoO_3 films.

Figs. 2(a), 2(b), 2(c) and 2(d) show the 2D AFM images of the pristine and Co-doped MoO_3. From these images, the surface seems to be rougher and more textured for the undoped sample. The root mean square (RMS) roughness values are summarized in Table II. RMS decreases with increasing Co-doping levels. Likewise, as shown in Fig. 2, the surface is formed by microplates elongated along the

substrate and separated by voids (dark areas in the AFM images). The shape and the size of the micro-plates are depending on the doping concentration. The size of the microplates is in correlation with the Co-doping level and increase uniformly with the Co concentration.

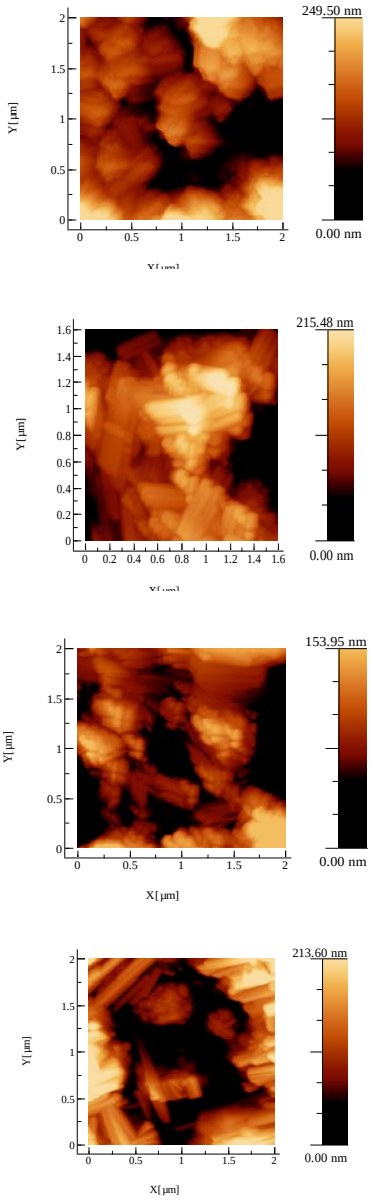

Fig. 2. 2D AFM images reflecting the formation of micro-plates on the surface of MoO_3 thin films synthesized on glass substrate: (a): undoped MoO_3, (b): 0.5 % of Co-doping, (c): 0.75 % of Co-doping and (d): 1 % of Co-doping.

TABLE II: RMS ROUGHNESS DETERMINED FROM AFM IMAGES

	Pure MoO_3	Co-MoO_3 (0.5%)	Co-MoO_3 (0.75%)	Co-MoO_3 (1%)
Rms (nm)	62.37	58.15	53.97	47.86

B. Photoluminescence Analysis

The photoluminescence is carried out at room temperature to complete the study of the optical properties of Co-doped MoO_3 nanofilms. The PL spectra are shown in Fig. 3.

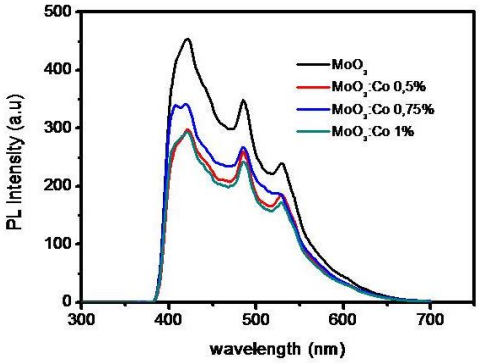

Fig. 3. PL spectra of MoO_3:Co thin films.

The fitting of PL spectra (Figs. 4 (a), (b), (c) and (d)) permits to evidence eight peaks located at around 400, 415, 440, 470, 487, 502, 527 and 537nm. Two peaks related to the blue and green emissions are very intense. At first glance, one notes that the photoluminescence response is very sensitive to Co-doping because the PL signal decreases with Co-doping. The presence of diverse defects in MoO_3 nanofilms could be sensitive to Co-doping.

Fig. 5 schematizes the mechanisms of the different emissions relating to the peaks determined by the fitting of the PL spectra. From this figure, the emissions located around 400 (3.10 eV) and 416 nm (2.98 eV) are due to band-to-band transitions. The peaks recorded at 439 nm (2.83 eV), 470 nm (2.64 eV) and at 487 nm (2.55 eV) are attributed to the exciton recombination between the electron localized at the interstitial molybdenum (Mo_i) and the holes in the valence band. Indeed, MoO_3 nanofilms are not stoichiometric and therefore contain some oxygen deficiencies. The samples are probably in the forms Mo_xO_{3x-1} such as MoO_2, Mo_2O_5, Mo_3O_8 and Mo_4O_{11}.

The green emission at 502 nm (2.47 eV) results from the electron transition from the ionized oxygen vacancies energy level to the valence band. The two emissions lines around 527 nm (2.35 eV) and 537 nm (2.31 eV) are explained in terms of transitions from the conduction band to the defect levels of O_{Mo} and O_i, respectively.

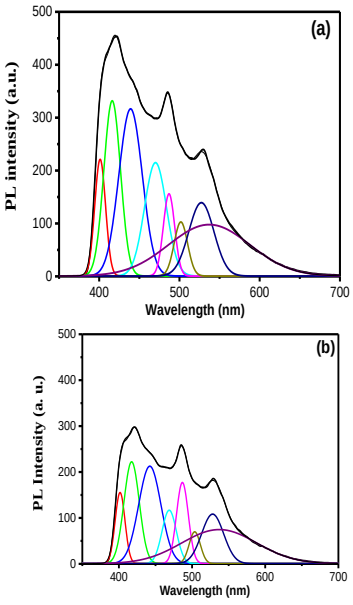

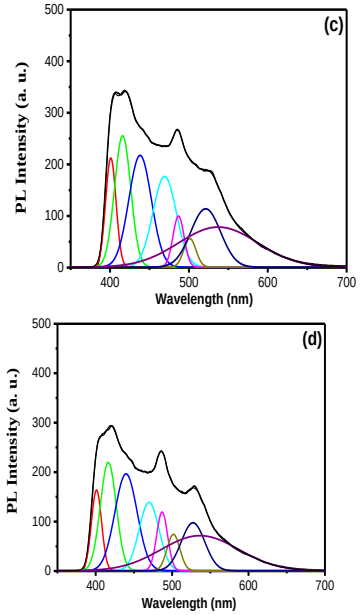

Fig. 4. Fitting of PL spectra in Gaussian form.

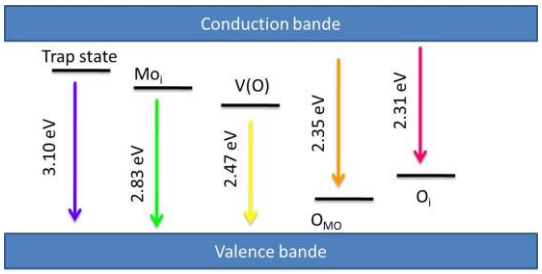

Fig. 5. Schematic diagram of the mechanism of the photoluminescence.

C. The Magnetic Properties Of Co-MoO_3 Nanofilms

The magnetic properties of sprayed Co-doped MoO_3 nanofilms were analyzed through the study of their hysteresis. Fig. 6 shows magnetization (*M-H*) curves measured by the VSM at room temperature. For all samples, ferromagnetic hysteresis shapes were observed, even for the undoped MoO_3.

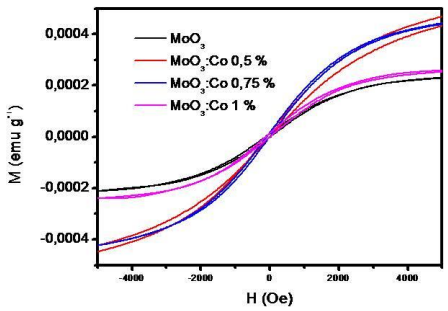

Fig. 6. M–H loops of pure and Co-doped MoO_3 thin films.

Magnetic properties of Co-doped MoO_3 such as Coercivity (Hc), the Magnetization (Ms) and Retentivity (Mr) values are listed in Table III.

These values show the effect of the cobalt in the MoO_3 matrix, but also the particularity of the doping at 0.5%: this is in agreement with the findings obtained from the structural study.

Cobalt has a known ferromagnetic behavior; this means that the ferromagnetism of Co-MoO_3 nanofilms is related to both cobalt doping and oxygen vacancies. Indeed, it was reported that the MoO_3 is not an intrinsically ferromagnetic material but rather a paramagnetic one [41]. This property is related to the +4 valence of molybdenum (Mo^{4+}). The Mo-O oxide containing oxygen vacancies is not stoichiometric with a chemical formula probably of the Mo_xO_{3x-1} form. The extrinsic behavior effect linked to the doping is probably related to the ferromagnetic character of cobalt and to a possible magnetic phase transition: by modification of the spin lattice is caused by the substitution of molybdenum by cobalt (Mo = [Kr] $4d^{10}5s^1$; Co = [Ar] $4s^2$ $3d^7$). This may explain the increase in magnetic defects in terms of the spin system.

TABLE III: COERCIVITY VALUES (HC), MAGNETIZATION (MS) AND RETENTIVITY (MR) OF CO-MoO_3 NANOFILMS

	Ms (10^{-4} emu)	Mr (10^{-6} emu)	Hc (Oe)
Pristine MoO_3	2.96	8.10	56.38
Co-MoO_3 (0.5%)	6.31	14.70	51.6
Co-MoO_3 (0.75%)	5.60	8.68	177.92
Co-MoO_3 (1%)	2.85	7.56	70.28

D. Photocatalytic Activity Testing

Fig. 7 (a to d), show the decrease of the absorption signal when the Co-MoO_3 nanofilms samples were submitted to UV irradiation: this clearly indicates the photodegradation of Methylene Blue (MB). The intensity of the most pronounced peak around 660 nm decreases with the irradiation time.

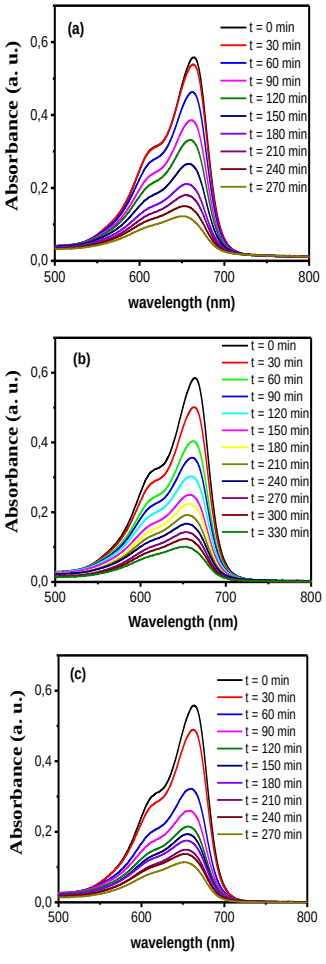

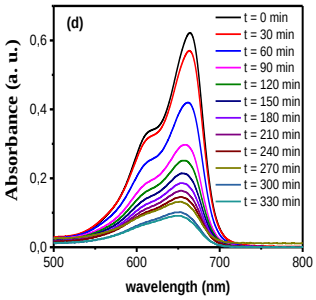

Fig. 7. The degradation of the Methylene Blue absorption in the presence of the MoO_3 samples. (a) Pristine MoO_3, (b), (c) and (d) Co-doped MoO_3 for Co-concentrations 0.5, 0.75 and 1%.

The observation of the photocatalytic effects can be described by the following mechanisms: at first, when MoO_3 nanofilms are illuminated by UV light with energy excitation greater than the gap, the electrons move from the valence band to the conduction band, electron-hole pairs are then created. The hydroxides groups present on the surface, created by the effect of UV-irradiation react with the photogenerated hole to produce O-H radicals and peroxide groups (O_2^-). The interaction of the peroxides with the protons forms a superoxide (HO_2^-) followed by the formation of hydrogen peroxide ($H_2O_2^-$). Secondly, a hydroxide radical may be occurring by etching an electron photogenerated with hydrogen peroxide. These reactive radicals and intermediate species react with the solution dye and degrade it into non-toxic organic compounds. This mechanism is illustrated by the following reactions:

$$MoO_3 + h\nu \rightarrow MoO_3 + e^- + h \quad (3)$$

$$OH^- + h^+ \rightarrow OH^* \quad (4)$$

$$O_2 + e^- \rightarrow O^-_2 \quad (5)$$

$$O_2^- + H^+ \rightarrow HO_2 \quad (6)$$

$$2HO_2 \rightarrow H_2O_2 + O_2 \quad (7)$$

$$H_2O_2 + e^- \rightarrow OH^- + OH^- \quad (8)$$

In addition to this analysis, the variation of the MB relative concentration (C/C_0) was studied against UV exposure time: Fig. 8 shows the C/C_0 and $1 - C/C_0$ variations where C is the MB concentration at the irradiation time (t) and C_0 is the concentration of the dye before irradiation. After 300 minutes of UV light irradiation, more than 80% of MB is degraded in the presence of Co-doped MoO_3 nanofilms. This shows that Co-MoO_3 nanofilms can be considered as an effective photocatalyst for the degradation of MB dyes. This evolution can be modeled by a law describing a first order kinetic reaction:

$$C = C_0 e^{-kt} \quad (9)$$

where k is the kinetic constant and C_0 is the initial concentration.

The calculated kinetic constant values are given in Table IV: the k parameter increases with the Co-doping level. As a complement to this observation, the photodegradation of MB was monitored through the normalized change in its concentration using degradation efficiency. The intersection of C/C_0 and $1 - C/C_0$ curves in Fig. 8 gives the half reaction time ($t_{1/2}$) of the MB degradation.

From Table IV, the half reaction time values decrease with cobalt doping concentration. The cobalt doping seems to improve the MB photocalysis phenomenon. In comparison with TiO_2, the kinetic constant of MoO_3 is smaller than 0.9 min^{-1} obtained by Lu *et al* [42]. If TiO_2 is considered as a suitable material for photocatalytic applications, α-MoO_3 comes as a competitor for theses applications. MoO_3 presents the advantage of being easily synthesized in thin films in its α-MoO_3 stable phase.

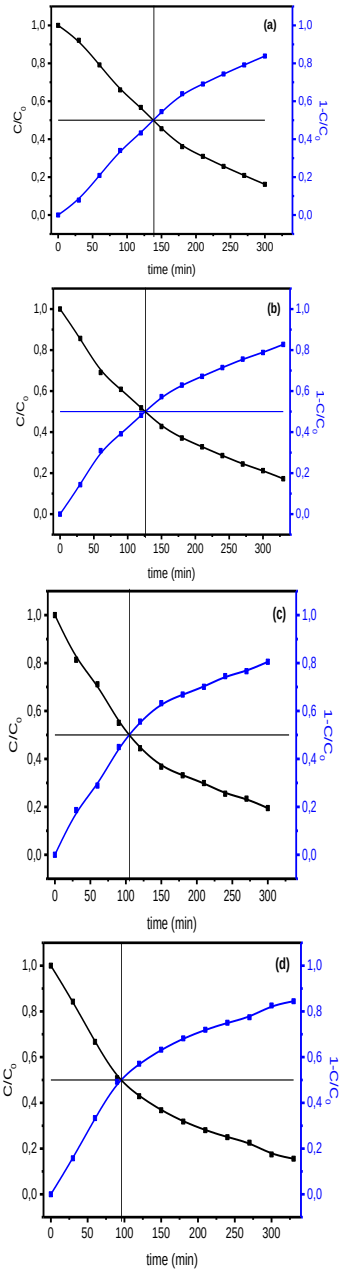

Fig. 8. Variation of concentration ratios of C/C_0 and $1 - C/C_0$. (a) Pristine MoO3, (b), (c) and (d) Co-doped MoO3 for Co-concentrations 0.5, 0.75 and 1%.

TABLE IV: KINETIC CONSTANTS AND HALF TIME REACTION VALUES OF MB SOLUTION DEGRADATION

	Pure MoO_3	Co-MoO_3 (0.5%)	Co-MoO_3 (0.75%)	Co-MoO_3 (1%)
k (10^3 mn^{-1})	3.77	6.08	7.92	8.38
$t_{1/2}$ (min)	138	126	104	96

IV. Conclusion

Some physical properties of pure and Co-doped MoO_3 synthesized on glass substrates by the spray pyrolysis method have been reported and discussed. The orthorhombic structure of the samples is confirmed by X-ray diffraction showing the principal orientations according to (020) and (040) directions. AFM measurements indicate that MoO_3 surface is rough and formed by micro-plates whose sizes are depending on Co-doping concentrations. Optical properties are investigated through the reflectance, the transmittance spectra and photoluminescence. Magnetic measurements using Vibrating Sample Magnetometer (VSM) unit show hysteresis loops leading to a ferromagnetic behavior of Co-MoO_3 thin films. Photocatalytic degradation of aqueous solution of methylene blue observed under UV irradiation in the presence of Co-MoO_3 nanofilms shows that more than 80% of methylene blue was degraded.

Acknowledgement

The authors thank infinitely and sincerely Prof. Didier Tonneau for his help and contribution in some experimental measurements.

References

[1] R. Singh, M. Kumar, M. Saini, A. Singh, B. Satpati, and T. Som, "Growth of TiO_2 thin films on chemically textured Si for solar cell applications as a hole-blocking and antireflection layers," *Appl. Surf. Sc.*, vol. 418, pp. 225–231, 2017.

[2] P. Madhukar, D. S. Jyothi, N. Jayababu, and M. V. R. Reddy, "Annealing temperature on the structural and dielectric properties of WO_3 thin films," *Materials Today: Proceedings*, vol. 3, pp. 4199–4204, 2016.

[3] A. Boukhachem, C. Bouzidi, R. Boughalmi, R. Ouerteni, M. Kahlaoui, M. Ouni, H. Elhouichet, and M. Amlouk, "Physical investigations on MoO_3 sprayed thin film for selective sensitivity applications," *Ceramics International*, vol. 40, pp. 13427–13435, 2014.

[4] R. Murugan, G. Vijayaprasath, T. Mahalingam, and G. Ravi, "Room temperature ferromagnetism of Ni doped cesium oxide single crystalline thin Films deposited by using rf magnetron sputtering," *Materials Letters*, vol. 162, pp. 71–74, 2016.

[5] M. Zhang, T. Xue, S. Xu, Z. Li, Y. Yan, and Y. Y. Huang, «Giant field-induced strain in $Nb2O_5$-modified $(Bi_{0.5}Na_{0.5})_{0.94}Ba_{0.06}TiO_3$ lead-free ceramics," *Ceramics International*, vol. 43, pp. 5842-5846, 2017.

[6] O. Krško, T. Plecenik, T. Roch, B. Grančič, L. Satrapinskyy, M. Truchlý, P. Ďurina, M. Gregor, P. Kúš, and A. Plecenik, "Flexible highly sensitive hydrogen gas sensor based on a TiO_2 thin film on polyimide foil," *Sensors and Actuators, B: Chemical*, vol. 240, pp. 1058-1065, 2017.

[7] J. Shen, S. Guo, C. Chen, L. Sun, S. Wen, Y. Chena, and S. Ruan, "Synthesis of Ni-doped -MoO_3 nanolamella and their improved gas sensing properties," *Sensors and Actuators B*, vol. 252, pp. 757–763, 2017.

[8] L. Zhang, Z. Liu, L. Jin, B. Zhang, H. Zhang, M. Zhu, and W. Yang, "Self-assembly gridding-MoO_3 nanobelts for highly toxic H_2S gas sensors," *Sensors and Actuators B: Chemical*, vol. 237, pp. 350-357, 2016.

[9] A. V. Emeline, X. Zhang, T. Murakami, and A. Fujishima, "Highly stable and efficient Ag/AgCl-TiO_2 photocatalyst: Preparation, characterization, and application in the treatment of aqueous hazardous pollutant," *Journal of Hazardous Materials*, vol. 211-212, pp. 154–160, 2012.

[10] N. Tripathy, R. Ahmad, H. Kuk, D. H. Lee, Y. B. Hahn, and G. Khang, "Highly stable hydrazine chemical sensor based on vertically-aligned ZnO nanorods grown on electrode," *Journal of Photochemistry & Photobiology, B: Biology*, vol. 161, pp. 312–317, 2016.

[11] M. N. Gururaj, A. Oki, and Z. Luo, "Efficient photocatalysts for degradation of rhodamine B," *Journal of Colloid and Interface Science*, vol. 430, pp. 257–264, 2014.

[12] Z. Li, G. H. Wang, C. Liang, and A. Zhang, "Sputtered gold-coated ITO nanowires by alternating depositions from Indium and ITO targets for application in surface-enhanced Raman scattering," *Applied Surface Science*, vol. 347, pp. 541–547, 2015.

[13] G. S. Zakharova, C. Täschner, V. L. Volkov, I. Hellmann, R. Klingeler, A. Leonhardt, and B. Büchner, "MoO3-δ nanorods: Synthesis, characterization and magnetic properties," *Solid State Sci*, vol. 9, pp. 1028–1032, 2007.

[14] H. Sinaim, D. J. Ham, J. S. Lee, A. Phuruangrat, S. Thongtem, and T. Thongtem, "Electrochemical performance and stability of co-deposited pd-au on phase-pure tungsten carbide for hydrogen oxidation link," *Journal of Alloys Compounds*, vol. 516, pp. 172-178, 2012.

[15] W. Pan, R. Tian, H. Jin, Y. Guo, L. Zhang, X. Wu, L. Zhang, Z. Han, G. Liu, J. Li, G. Rao, H. Wang, and W. Chu, "Flower-like hierarchical h-MoO3: New findings of efficient visible light driven nano photocatalyst for methylene blue degradation," *Chem. Mat.*, vol. 22, pp. 6202–6208, 2010.

[16] Z. Wu, D. Wang, X. Liang, and A. Sun, "Flower-like hierarchical h-MoO3: new findings of efficient visible light driven nano photocatalyst for methylene blue degradation," *Ultrason. Sonochem*, vol. 18, pp. 288–292, 2011.

[17] O. Kamoun, A. Boukhachem, M. Amlouk, and S. Ammar, "Physical study of Eu doped MoO_3 thin films," *Journal of Alloys and Compounds*, vol. 687, pp. 595-603, 2016.

[18] M. T. Qamar, M. Aslam, Z. A. Rehan, M. T. Soomro, I. Ahmad, M. Ishaq, I. M. I. Ismail, P. Fornasiero, and A. Hameed, "Synthesis, characterization, and sunlight mediated photocatalytic activity of CuO Coated ZnO for the removal of nitrophenols," *Chemical Engineering Journal*, vol. 7, pp. 8757-8768, 2015.

[19] B. Sanga, Y. Nagoyab, K. Kushiyab, and O. Yamase, "Physical investigations on MoO_3 sprayed thin film for selective sensitivity applications," *Sol. Energy Mat. Sol. Cells*, vol. 75, p. 179, 2003.

[20] Q. Fu, L. Hu, D. Yu, J. Sun, H. Zhang, B. Huo, and Z. Zhao, "ZnO thin films deposited by a CVT technique in closed ampoules," *Mat. Lett.*, vol. 63, pp. 316-318, 2009.

[21] T. Shimomura, D. Kim, and M. Nakayama, "Optical properties of high-quality ZnO thin films grown by a sputtering method," *J. Lumin.*, vol. 112, pp. 191-195, 2005.

[22] M. N. R. Henley, "The growth of transparent conducting ZnO films by pulsed laser ablation," *Surf. Coat. Technol.*, vol. 177–178, pp. 271-276, 2004.

[23] J. L. VanHeerden and R. Swanepoel, "XRD analysis of ZnO thin films prepared by spray pyrolysis," *Thin Solid Films*, vol. 1–2, pp. 72-77, 1997.

[24] W. T. Seeber, M. O. Abou-Helal, S. Bartha, D. Beil, T. Ho Eche, H. Afify, and S. E. Demian "Transparent semiconducting ZnO:Al thin films prepared by spray pyrolysis," *Mater. Sci. Semicond. Process*, vol. 2, pp. 45-55, 1999.

[25] R. Ayouchi, D. Leinen, F. Martın, M. Gabas, E. Dalchiele, and J. R. Ramos- Barrado, "Preparation and characterization of transparent ZnO thin films obtained by spray pyrolysis," *Thin Solid Films*, vol. 426, pp. 68-77, 2003.

[26] A. Ashour, M. A. Kaid, N. Z. El-Sayed, and A. A. Ibrahim, "Physical properties of ZnO thin films deposited by spray pyrolysis technique," *App. Surf. Sci*, vol. 252, pp. 7844-7848, 2006.

[27] A. Boukhachem, O. Kamoun, C. Mrabet, C. Mannai, N. Zouaghi, A. Yumak, K. Boubaker, and M. Amlouk, "Structural, optical, vibrational and photoluminescence studies of Sn-doped MoO_3 sprayed thin films," *Mat. Res. Bul.*, vol. 72, pp. 252–263, 2015.

[28] K. Boubaker, A. Chaouachi, M. Amlouk, and H. Bouzouita, "Enhancement of pyrolysis spray disposal performance using thermal time-response to precursor uniform deposition," *Eur. Phys. J. Appl. Phys.*, vol. 37, pp. 105-109, 2007.

[29] A. Boukhachem, M. Mokhtari, N. Benameur, A. Ziouche, M. Martínez, P. Petkova, M. Ghamnia, A. Cobo, M. Zergoug, and M. Amlouk, "Structural optical magnetic properties of Co doped α-MoO_3 sprayed thin films," *Sensors and Actuators A*, vol. 253, pp. 198–209, 2017.

[30] Z. Li, W. Wang, Z. Zhao, X. Liu, and P. Song, "Facile synthesis and enhanced trimethylamine sensing performances of W-doped MoO_3 nanobelts," *Materials Science in Semiconductor Processing*, vol. 66, pp. 33–38, 2017.

[31] P. Ren, X. Liu, K. Zhang, P. Zhang, F. Teng, Z. Zhang, E. Xie, and P. Yan, "Green photoluminescence from erbium-doped molybdenum trioxide," *Mat. Lett.*, vol. 122, pp. 320-322, 2014.

[32] S. Yang, Y. Liu, T. Chen, W. Jin, T. Yang, M. Cao, S. Liu, J. Zhou, G. S. Zakharova, and W. Chen, "Zn doped MoO_3 nanobelts and the enhanced gas sensing properties to ethanol," *App. Surf. Sci.*, vol. 393, pp. 377-384, 2017.

[33] S. Baia, C. Chena, D. Zhangb, R. Luoa, D. Lia, A. Chena, and C. C. Liu, "Intrinsic characteristic and mechanism in enhancing H_2S sensing of Cd-doped α-MoO_3 nanobelts," *Sens. Actuators B*, vol. 204, pp. 754-762, 2014.
[34] W. Yu, X. Liu, P. Likun, J. Li, J. Liu, J. Zhang, P. Li, C. Chen, and Z. Sun, "Enhaced visible light photocatalytic degradation of methylene blue by F-doped TiO_2," *Appl. Surf. Sc.*, vol. 319, pp. 107-112, 2014.
[35] A. Matos, J. Laine, J. M. Herrmann, D. Uzcategui, and J. L. Brito, "Influence of activated carbon upon titania on aqueous photocatalytic consecutive runs of phenol photodegradation," *Applied Catalysis B: Environmental*, vol. 70, pp. 461–469, 2007.
[36] Y. Liu, P. Feng, Z. Wang, X. Jiao, and F. Akhtar, "Novel fabrication and enhanced photocatalytic MB degradation of hierarchical porous monoliths of MoO_3 nanoplates," *Nanoplates. Scientific Reports*, vol. 7, no. 1, p. 1845, 2017.
[37] M. Szkodaa, K. Trzcinski, K. Siuzdak, and A. Lisowska-Oleksiak, "Photocatalytical properties of maze-like MoO_3 microstructures prepared by anodization of Mo plate," *Electrochimica Acta*, vol. 228 pp. 139–145, 2017.
[38] M. Szkoda, K. Trzciński, M. Kleinb, and K. Siuzdak, "Lisowska-Oleksiaka A., The influence of photointercalaction and photochromism effects on the photocatalytic properties of electrochemically obtained maze-like MoO_3 microstructures," *Separation and Purification Technology*, vol. 197, pp. 382–387, 2018.
[39] A. Chithambararaj, N. S. Sanjini, S. Velmathi, and B. A. Chandra, "Preparation of h-MoO3 and a-MoO_3 nanocrystals: Comparative study on photocatalytic degradation of methylene blue under visible light irradiation," *Phys. Chem. Chem. Phys.*, vol. 15, no. 35, pp. 14761–14769, 2013.
[40] Y. Chen, C. L. Lu, L. Xu Y. Ma, W. Hou, and J. J. Zhu, "Single-crystalline orthorhombic molybdenum oxide nanobelts: synthesis and photocatalytic properties," *Cryst Eng Comm*, vol. 12, no. 11, pp. 3740-3747, 2010.
[41] U. Hisashi, T. Naoyuki, and K. Minoru, "The reactivities and the stabilities of the paramagnetic species formed on the surface of Al_2O_3, MoO_3, CoO and SiO_2," *J. Less. Common. Mat.*, vol. 36, pp. 387-394, 1974.
[42] Z. Lu, F. Chen, M. He, M. Song, Z. Ma, W. Shi, Y. Yan, J. Lan, F. Li, and P. Xiao, "Microwave synthesis of a novel magnetic imprinted TiO_2 photocatalyst with excellent transparency for selective photodegradation of enrofloxacin hydrochloride residues solution," *Chemical Engineering Journal*, vol. 249, pp. 15–26, 2014.

Nadir Benameur is an associate professor in the Department of Biology and a researcher at the laboratory of condensed matter sciences at Universit é Oran 1 Ahmed Ben Bella, 31100, Oran Algeria. He works in the field of the characterization of large-gap semiconductor materials.

Abdelwahab Boukhachem is a lecturer at the Faculty of Sciences of Tunis El-Manar University and researcher at the unit of physics of semiconductors devices of Tunis University, 2092 Tunis, Tunisia.

Mostefa Ghamnia is a doctor professor at Universit é Oran 1 Ahmed Ben Bella, 311000, Oran, Algeria. He is a head of the Laboratory of Condensed Matter Sciences (LSMC). He has supervised several doctoral theses and has led numerous research projects in the framework of international cooperation

Mohamed Ali Chakhoum is a PhD student. His thesis is supervised by Prof. M. Ghamnia at the Laboratory of Condensed Matter Sciences (LSMC), Universit éOran 1, Ahmed Ben Bella, 31100, Oran, Algeria

Mohamed Amine Dahamni is a PhD student. His is supervised by Prof. M. Ghamnia at the Laboratory of Condensed Matter Sciences (LSMC), Universit éOran 1, Ahmed Ben Bella, 31100, Oran, Algeria. He works on the synthesize of TCO materials.

Carole Fauquet is lecturer and researcher at the Centre Interdisciplinaire de Nanoscience de Marseille, University of Marseille, Campus of Luminy, 13288, Marseille, France. She co-directed with professor M. Ghamnia the Algerian-French cooperation project Tassili MDU915 from 2014 to 2018.